Enhanced Stability of Nickel Phyllosilicate Anchored Ni/SiO_2 Catalyst for Liquid-Phase Hydrogenation and Hydrodeoxygenation

Honghui Ning [1,2,*], Zhiying Du [1,2], Chenglin Cai [1,2] and Shengchao Huang [1,2,*]

[1] Hubei Three Gorges Laboratory, Yichang 443007, China; duzhiying@xingfagroup.com (Z.D.); caichenglin@xingfagroup.com (C.C.)
[2] Xinjiang Key Laboratory of Sulfide and Derivative Preparation, Aksu 843000, China

* Corresponding author. E-mail: ninghonghui@xingfagroup.com (H.N.); huangshengchao@xfjt.com (S.H.)

Received: 18 November 2025; Revised: 8 December 2025; Accepted: 19 January 2026; Available online: 26 January 2026

SUPPORTING FIGURES

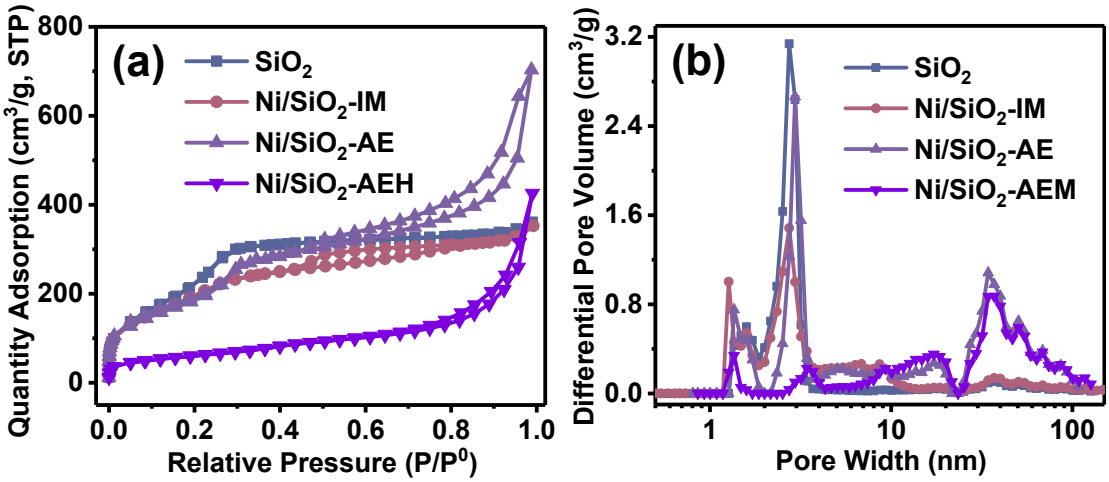

Figure S1. Textural characterization of SiO_2, Ni/SiO_2-IM, Ni/SiO_2-AE and Ni/SiO_2-AEH. (**a**) Adsorption-desorption isotherms and (**b**) pore size distributions.

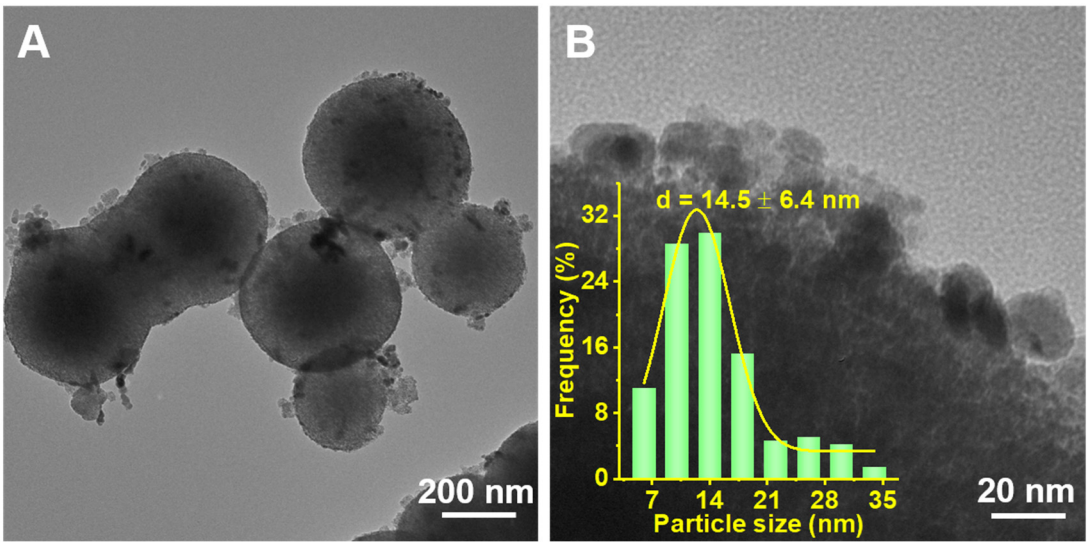

Figure S2. Characterization of Ni/SiO2-IM. (**a**) TEM image and (**b**) partial enlarged picture. *Inset* in (**b**) is the corresponding particle size distribution.

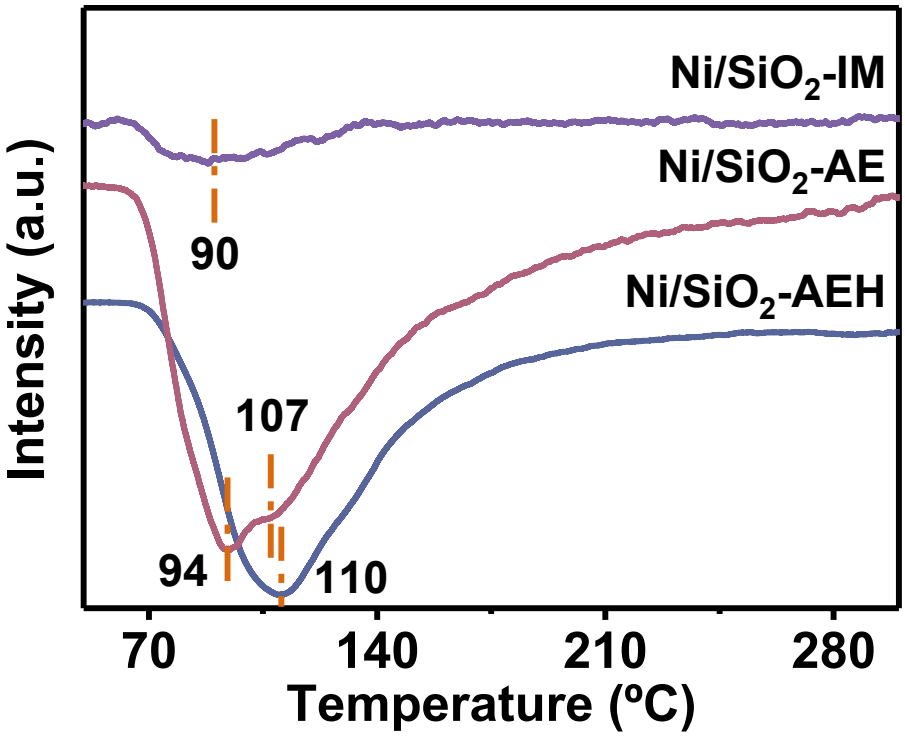

Figure S3. H2-TPD profiles of Ni/SiO2-IM, Ni/SiO2-AE and Ni/SiO2-AEH.

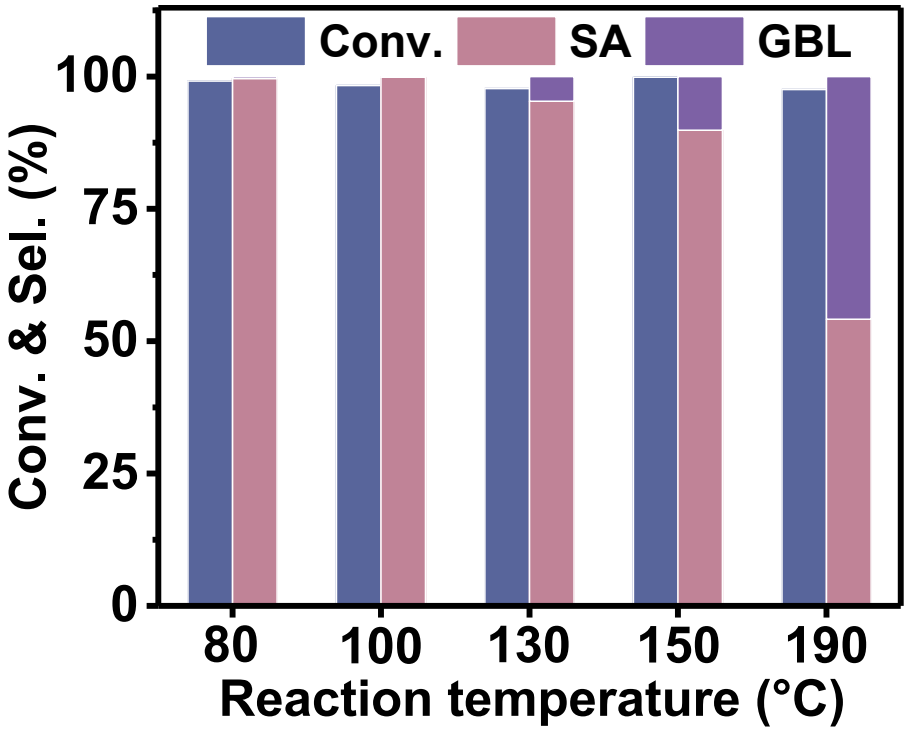

Figure S4. Catalytic performance of Ni/SiO_2-AEH versus reaction temperature (0.2 g MA, 10 mg Ni/SiO_2-AEH, 2.5 MPa H_2, 3 h).

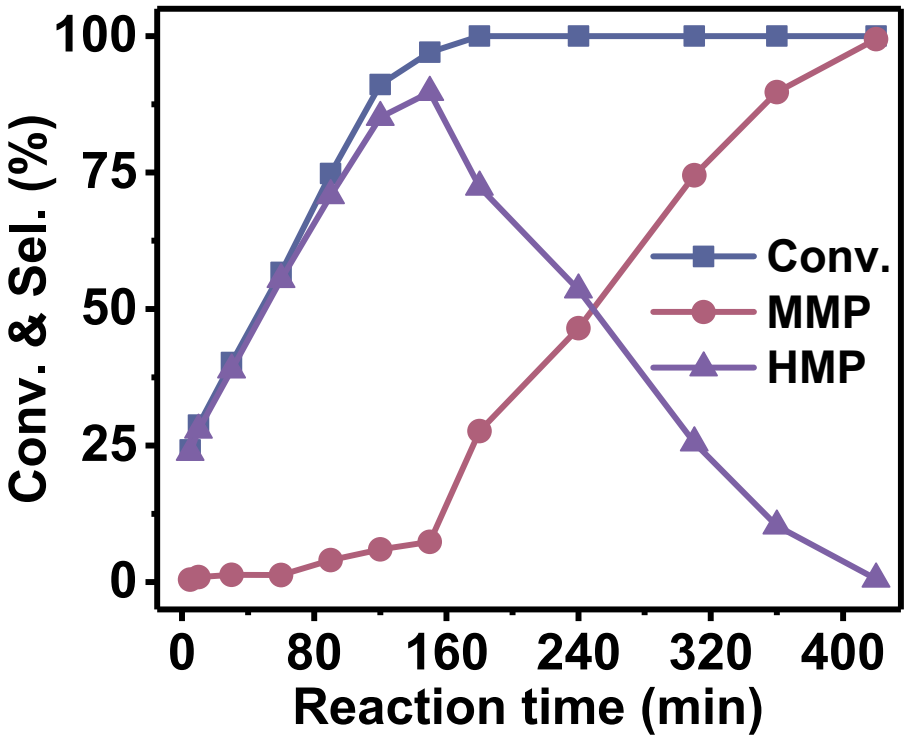

Figure S5. Time courses for the catalytic conversion of vanillin over Ni/SiO_2-AEH catalyst. Reaction conditions: 15 mg catalyst,152 mg vanillin, 10 ml dioxane, 100 °C, 2 MPa H_2.

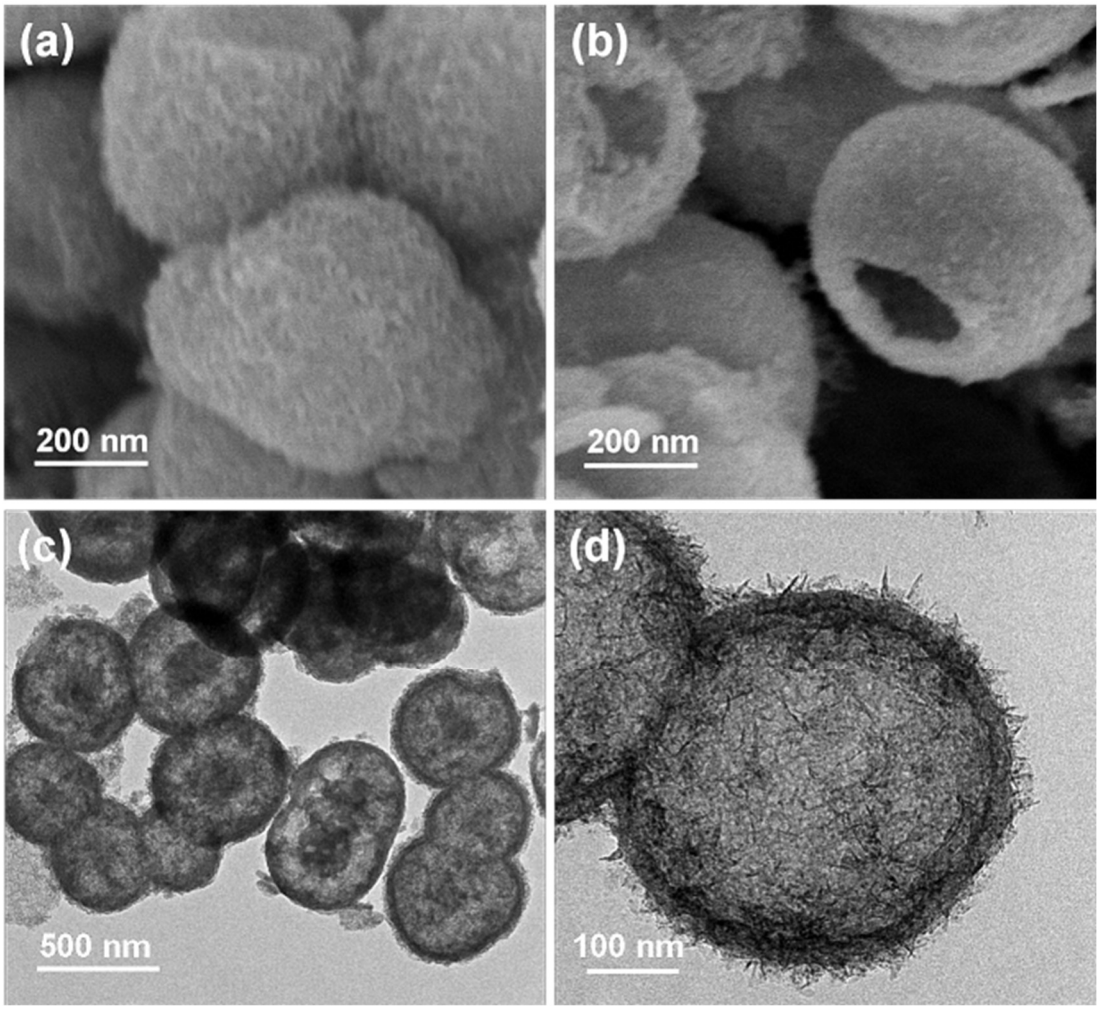

Figure S6. Morphology characterization of spent Ni/SiO_2-AE and Ni/SiO_2-AEH catalysts: (**a**) SEM and (**c**) TEM images of Ni/SiO_2-AE after four runs; (**b**) SEM and (**d**) TEM images of Ni/SiO_2-AEH after six runs.

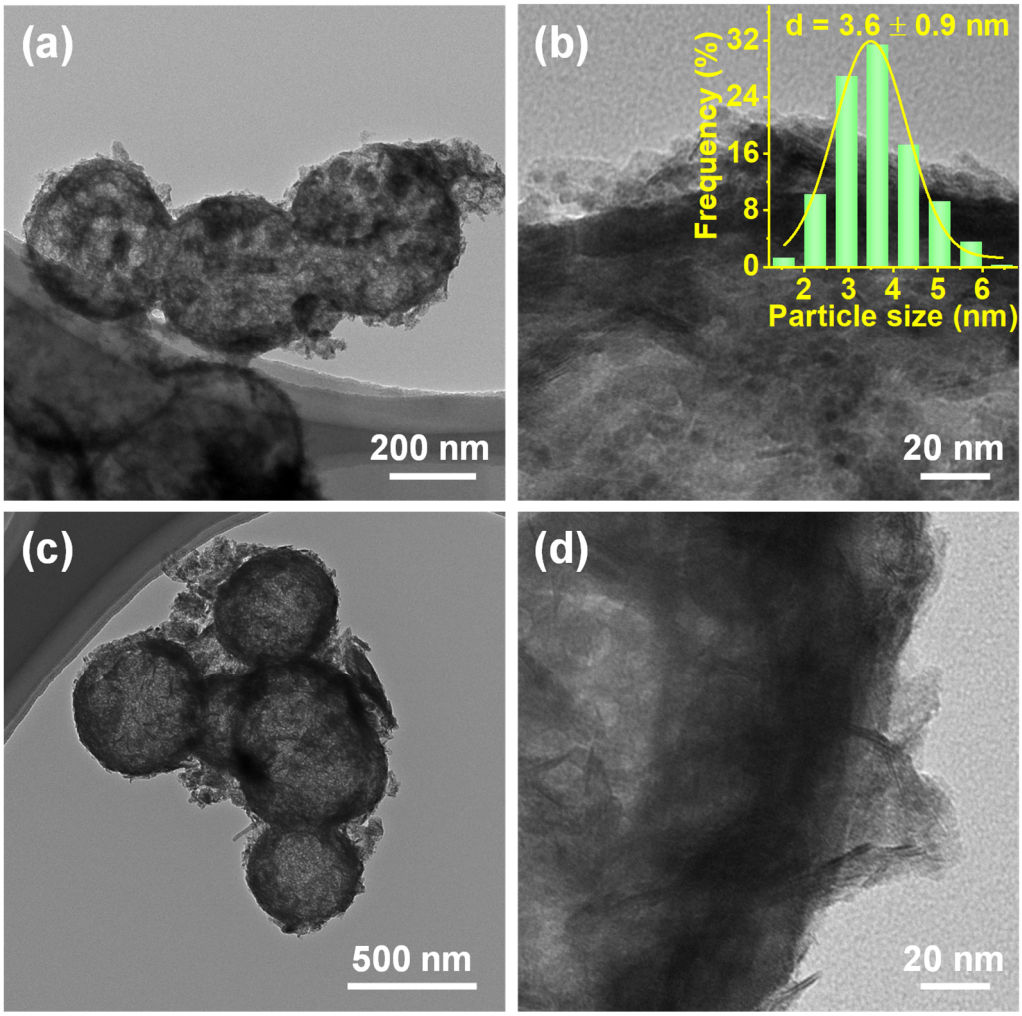

Figure S7. Characterization of fresh and spent Ni/SiO_2-AEH-800 catalyst. (**a**) TEM image and (**b**) partial enlarged picture of fresh Ni/SiO_2-AEH-800 catalyst; (**c**) TEM image and (**d**) partial enlarged picture of Ni/SiO_2-AEH-800 catalyst after three runs. *Inset* in (**b**) is the corresponding particle size distribution.

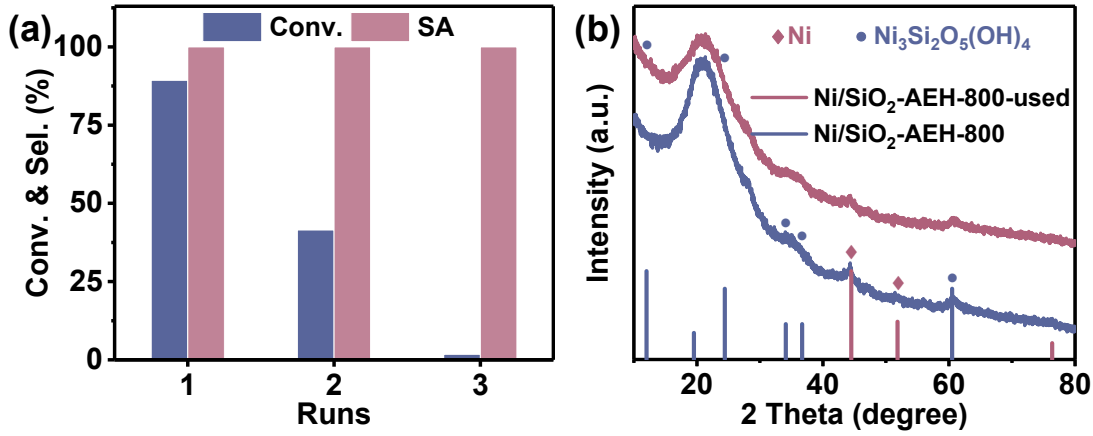

Figure S8. (**a**) Recycling test of the Ni/SiO_2-AEH-800 catalyst. Reaction condition: 10 mg catalyst, 250 mg MA, 2 ml 1,4-dioxane, 80 °C, 2.5 MPa H_2, 3 h. (**b**) XRD patterns of fresh and spent Ni/SiO_2-AEH-800 catalysts.

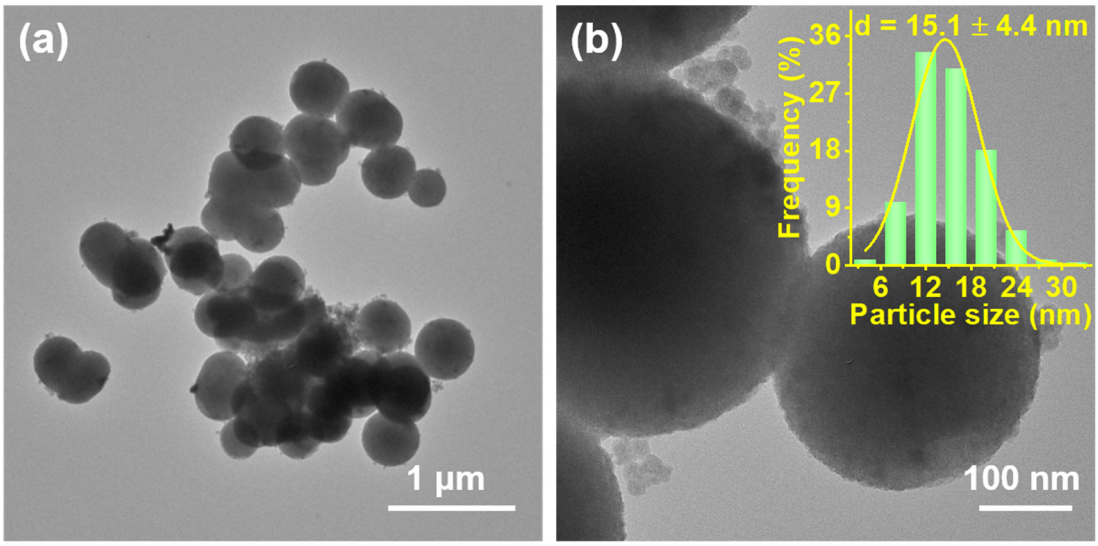

Figure S9. TEM images of Cu/SiO_2-IM (**a**,**b**). *Inset* in (**b**) is the particle size distribution.

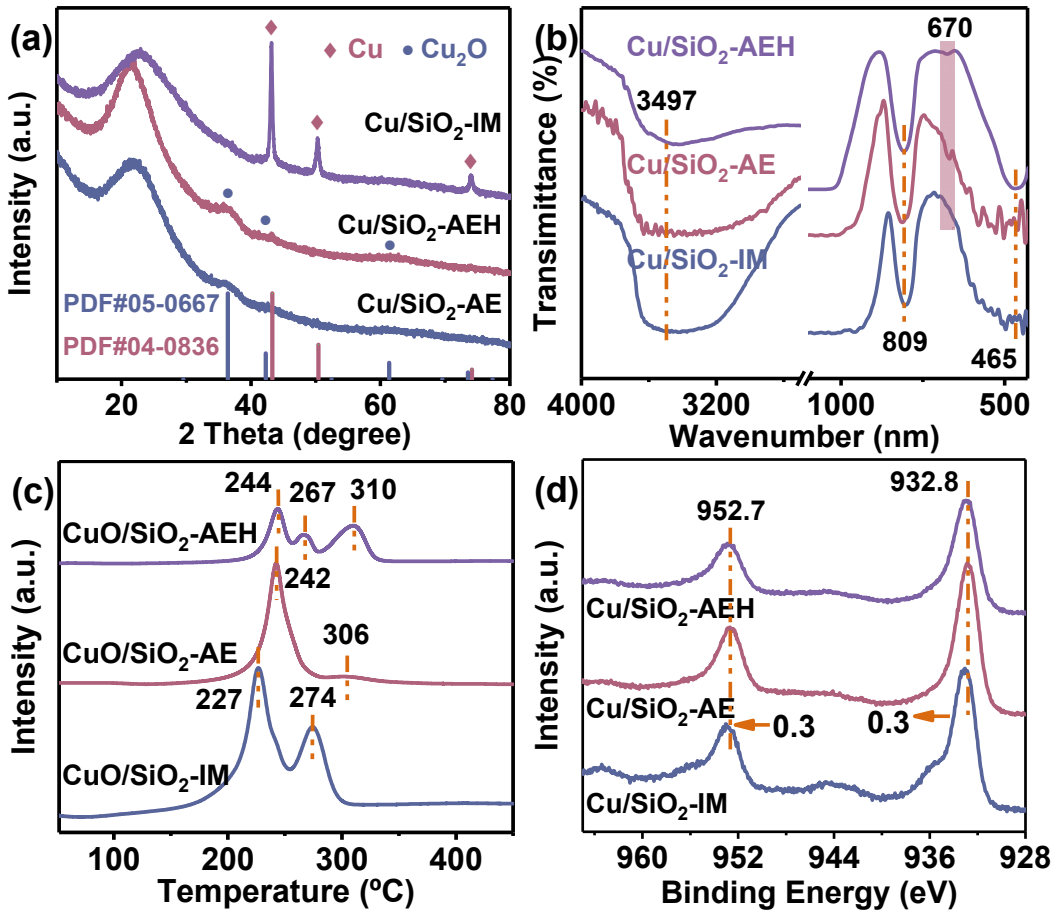

Figure S10. Physical characterization of Cu-based catalysts. (**a**) XRD patterns of Cu/SiO_2-IM, Cu/SiO_2-AE and Cu/SiO_2-AEH; (**b**) FT-IR spectra of Cu/SiO_2-IM, Cu/SiO_2-AE and Cu/SiO_2-AEH catalysts; (**c**) H_2-TPR profiles of CuO/SiO_2-IM, CuO/SiO_2-AE and CuO/SiO_2-AEH and (**d**) Cu 2p photoelectron spectrum of Cu/SiO_2-IM, Cu/SiO_2-AE and Cu/SiO_2-AEH catalysts.

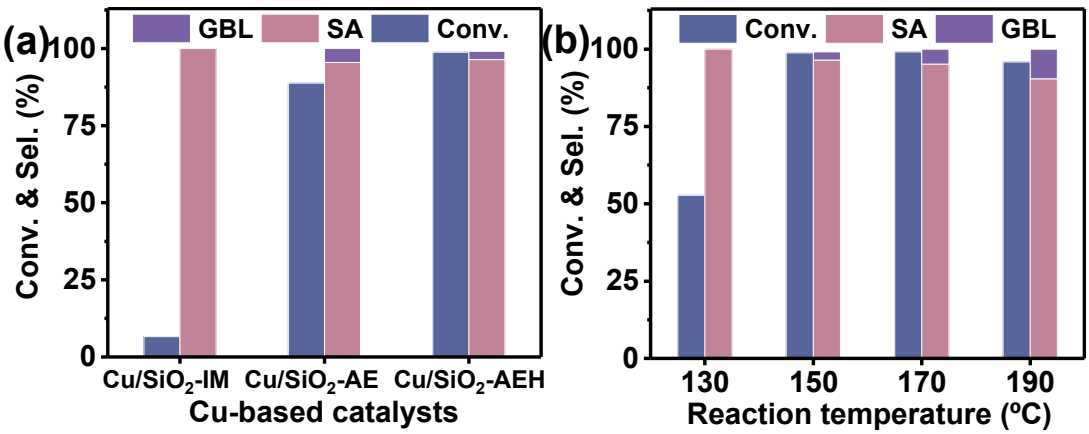

Figure S11. The hydrogenation performance of MA over Cu-based catalysts. (**a**) Catalytic evaluation of Cu/SiO_2, Cu/SiO_2-AE and Cu/SiO_2-AEH catalysts; Reaction conditions: 20 mg cat., 100 mg MA, 2 ml dioxane, 150 °C, 3 MPa H_2, 3 h. (**b**) Catalytic performance of Cu/SiO_2-AEH versus reaction temperature.

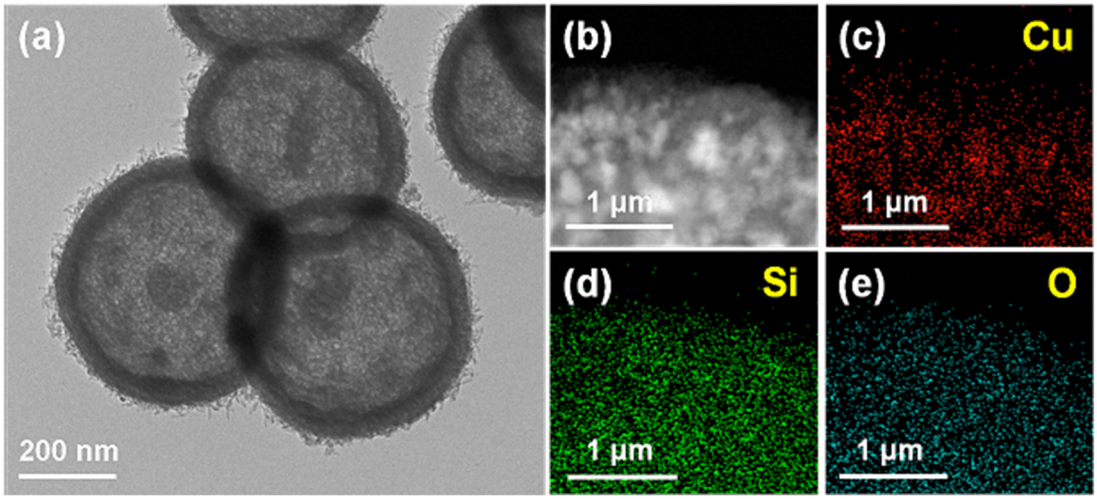

Figure S12. Electron microscopic characterization of Cu/SiO_2-AEH after fifth run. (**a**) TEM image, (**b**) HRTEM-HAADF image and (**c**–**e**) corresponding HRTEM-STEM mapping of Cu, Si and O.

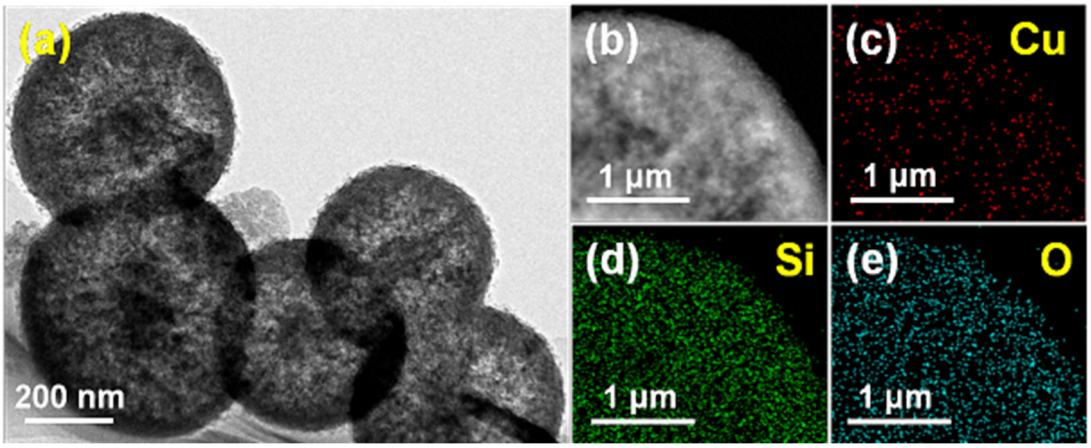

Figure S13. Electron microscopic characterization of Cu/SiO_2-AE after fifth run. (**a**) TEM image, (**b**) HRTEM-HAADF image and (**c**–**e**) corresponding HRTEM-STEM mapping of Cu, Si and O.

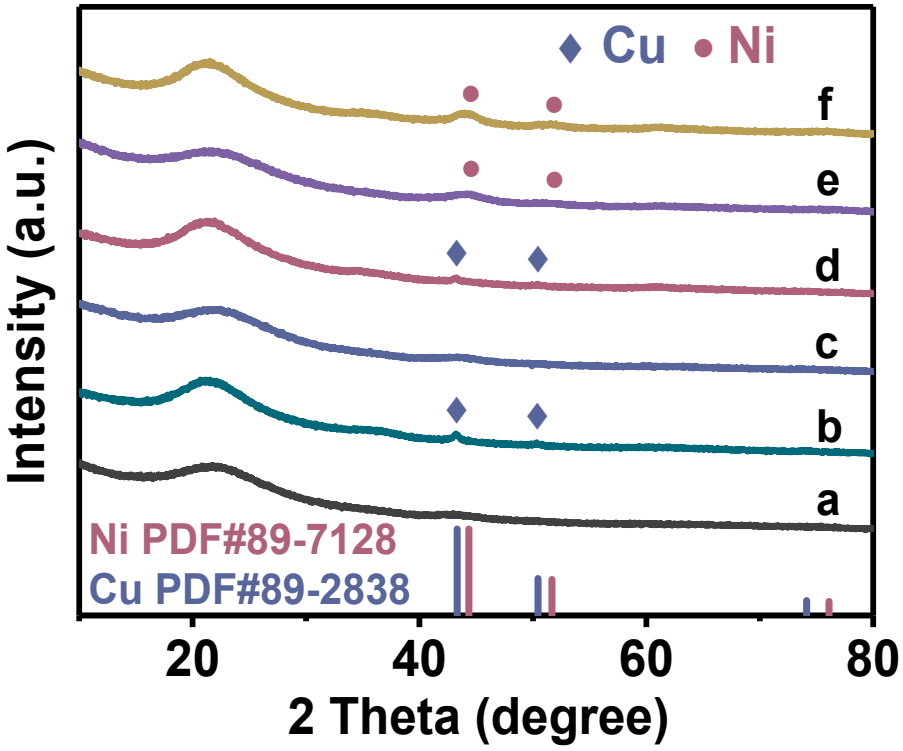

Figure S14. XRD patterns of (a) Cu_8Ni_2/SiO_2-AE, (b) Cu_8Ni_2/SiO_2-AEH, (c) Cu_5Ni_5/SiO_2-AE, (d) Cu_5Ni_5/SiO_2-AEH, (e) Cu_2Ni_8/SiO_2-AE and (f) Cu_2Ni_8/SiO_2-AEH.

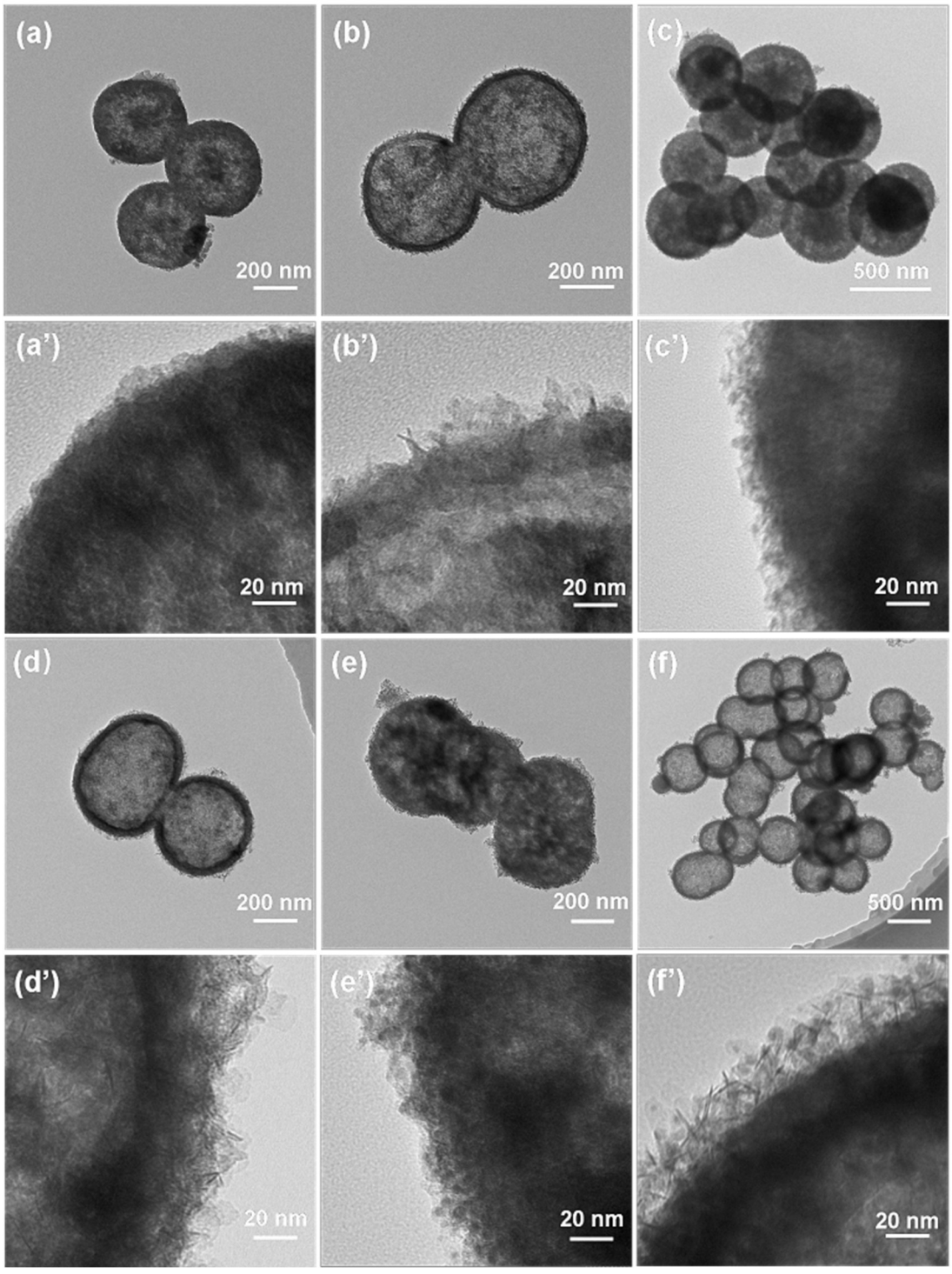

Figure S15. TEM images of (**a**) Cu_8Ni_2/SiO_2-AE; (**b**) Cu_8Ni_2/SiO_2-AEH; (**c**). Cu_5Ni_5/SiO_2-AE; (**d**) Cu_5Ni_5/SiO_2-AEH; (**e**) Cu_2Ni_8/SiO_2-AE and (**f**) Cu_2Ni_8/SiO_2-AEH and corresponding enlarged images (**a'**–**f'**).

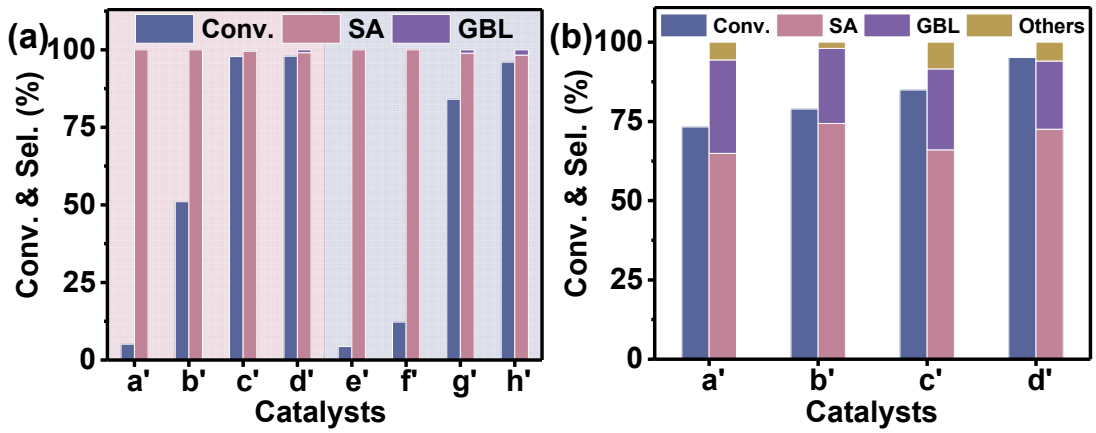

Figure S16. Reaction studies on MA hydrogenolysis. (**a**) Catalytic evaluation of (a') Cu_8Ni_2/SiO_2-AEH, (b') Cu_5Ni_5/SiO_2-AEH, (c') Cu_2Ni_8/SiO_2-AEH, (d') Ni/SiO_2-AEH, (e') Cu_8Ni_2/SiO_2-AE, (f') Cu_5Ni_5/SiO_2-AE, (g') Cu_2Ni_8/SiO_2-AE and (h') Ni/SiO_2-AE. Reaction conditions: 10 mg cat., 200 mg MA, 2 ml dioxane, 80 °C, 2 MPa H_2, 2.5 h. (**b**) Catalytic evaluation of (a') Cu_8Ni_2/SiO_2-AEH, (b') Cu_5Ni_5/SiO_2-AEH, (c') Cu_2Ni_8/SiO_2-AEH and (d') Ni/SiO_2-AEH. Reaction conditions: 10 mg cat., 200 mg MA, 2 ml dioxane, 200 °C, 2 MPa H_2, 2.5 h.

SUPPORTING TABLES

Table S1. BET surface areas and pore structure parameters of Ni-based catalysts.

Entry	Materials	S_{BET} (m^2/g)	Pore Size (nm)	Pore Volume (cm^3/g)
1	SiO_2	1011	2.4	0.56
2	Ni/SiO_2-IM	758.5	3.0	0.52
2	Ni/SiO_2-AE	802.0	5.2	1.07
3	Ni/SiO_2-AEH	219.6	11.1	0.66

Pore size: BJH Desorption average pore diameter; Pore Volume: BJH Desorption cumulative volume.

Table S2. Characterization of active metal Ni in as-synthesized catalysts.

Entry	Materials	Ni content (wt%) [a]	d_{Ni} (nm) [b]	Ni dispersion (%) [c]
1	Ni/SiO_2-IM	9.7	14.5	5.5
2	Ni/SiO_2-AE	9.1	4.0	26.5
3	Ni/SiO_2-AEH	8.9	3.3	35.1
4	Ni/SiO_2-AE-4 runs	4.5	3.9	24.2
5	Ni/SiO_2-AEH-6 runs	8.7	3.3	32.7

[a] Actual loading of Ni was determined by ICP; [b] The mean particle size of Ni was calculated by TEM images; [c] Measured by N_2O surface oxidation.

Table S3. O 1s binding energy and surface Ni oxides proportion of as-synthesized Ni based catalysts [a].

Catalysts	O 1s			$\Delta E_{Ni\text{-}Si}$ [b]	A_{Ni}/A_{Si} [c]
	NiO	1:1 NiPS	SiO_2		
Ni/SiO_2-IM	530.3 (11.5%)	-	532.7 (88.5%)	-	0.29
Ni/SiO_2-AE	530.5 (4.7%)	531.5 (9.7%)	532.6 (85.6%)	753.0	0.26
Ni/SiO_2-AEH	-	531.5 (20.3%)	532.7 (79.7%)	753.1	0.31
Ni/SiO_2-AE-4 runs	530.5 (1.6%)	531.7 (8.0%)	532.8 (90.4%)	753.4	0.27
Ni/SiO_2-AEH-6 runs	-	531.7 (18.8%)	532.7 (81.2%)	753.3	0.28

[a] Determined by XPS; [b] ΔE_{Ni-Si} = Ni $2p_{3/2}$ − Si 2p; [c] A_{Ni}/A_{Si} is the atomic ratio of Ni to Si calculated from XPS.

Table S4. Comparison of the catalytic performance of different reported MA hydrogenation catalysts.

Catalysts [a]	Temp./°C	P/MPa	t/h	S/C [c]	Solvent	Yield/%	TOF/h^{-1}	Refs.
Ni/SiO_2-AEH	80	2	2.5	134	1,4-dioxane	97.0	52	This work
Ni/SiO_2-AEH [b]	80	2	2.5	134	1,4-dioxane	97.0	147.8	This work
Ni/SiO_2-AE	80	2	2.5	132	1,4-dioxane	94.4	49.8	This work
Ni/SiO_2-IM	80	2	2.5	124	1,4-dioxane	10.2	5.1	This work
31.5%Ni-PS-0.48	80	5	3	31.0	Tetrahydrofuran	95	9.8	[1]
Raney Ni	80	2	2.5	59.9	acetic anhydride	99.8	23.9	[2]
Ni NPs	100	2.5	6	25.5	acetic anhydride	99.6	4.2	
1%Pd/Al_2O_3	100	2.1	2	532	Supercritical CO_2	57	151.6	[3]
5%Ni/TiO_2	100	4	6	100	Tetrahydrofuran	100	16.7	[4]
30%Ni/ZrO_2-SiO_2	120	6	3	94.1	Tetrahydrofuran	97.1	30.5	[5]
30%NiO_2/SiO_2	180	3	3	97.3	Tetrahydrofuran	99.3	32.2	
Ni/MOR[b]	210	4.5	0.67	635	1,4-dioxane	99	350	[6]
10%Cu/$CeO_{2-\delta}$	210	4	1	302.3	Tetrahydrofuran	32	96.7	
10%Co/$CeO_{2-\delta}$	210	4	1	284.7	Tetrahydrofuran	70	199.3	[7]
10%Ni/$CeO_{2-\delta}$	210	4	1	299.3	Tetrahydrofuran	98	293.3	
10%Ni/ZrO_2(P)	210	5	1	311.3	Tetrahydrofuran	100	311.3	[8]
10%Ni/ZrO_2(H)	210	5	1	312.3	Tetrahydrofuran	92	287.3	
10%Ni/CeO_2	210	4	1	293.3	Tetrahydrofuran	100	293.3	[9]
10%Ni/Al_2O_3	210	4	8	293.3	Tetrahydrofuran	87.5	32.1	
3%Ru-25%Ni/SiO_2	240	7	4	206.2	Tetrahydrofuran	71.4	36.8	[10]
Pd-Sn/SiO_2	240	5	4	299.3	1,4-dioxane	47	35.2	[11]

[a] Turnover frequency (TOF) = (total number of designed products moles per hour)/(total number moles of active metal). [b] TOF was calculated based on the number of surface metal atoms in the catalysts when the conversion of MA is less than 10%. [c] S/C represents the molar ratio of substrate to metal.

Table S5. Comparison of the catalytic performance of different reported vanillin HDO catalysts.

Catalysts [a]	Temp. /°C	P/MPa	t/h	S/C [d]	Solvent	Conv./%	Yield/%	TOF/h^{-1}	Refs.
Ni/SiO_2-AEH	110	2	2	43.3	1,4-dioxane	99.8	99.2	21.5	This work
Ni/SiO_2-AEH [b]	110	2	2	43.3	1,4-dioxane	99.8	99.2	64.6	This work
Ni/SiO_2-AE	110	2	2	42.4	1,4-dioxane	99.2	11.7	2.5	This work
HD-Ni/N-CMS	110	2	1	300	H_2O	5.2	4.8	14.6	[12]
	130	2	10	300	H_2O	98	98	29.4	
Ni/NHPC	120	2	3	19	ethyl acetate	100	98	6.2	[13]
Cu/AC-600	120	2	5	7.1	H_2O	99.9	93.1	1.3	[14]
$Ni_{0.5}Zn_{1.5}Al_1$-MMO	130	1	2	10	Methanol	99	98	4.9	[15]
Co_1/NC-(SBA)	140	1	3	30.8	H_2O + Methanol	100	99.2	10.3	[16]
Ni@NC-(SBA)	140	1	3	30.8	H_2O + Methanol	0	0	0	
Ni/T-Nb_2O_5@C_2-2	150	1	1	15.5	H_2O + Ethanol	99.9	96.6	15.0	[17]
Ni/hydrophobic silica	150	1.5	1	/	Pickering emulsion	99	99	/	[18]
CoNi/Al_2O_3-2 [c]	150	1	1	-	H_2O	100	98.9	1872	[19]
Ni/NCB-900	150	0.5	2	44	H_2O	74.4	26.3	5.8	[20]
Co/N_8G/CF	150	0.5	2	5.2	H_2O	99	98	2.5	[21]
	80	0.5	12		H_2O	99	23.8	0.1	
Co_xP@POP	150	4	5	3	isopropanol	100	65	0.4	[22]
Cu-Ni/CeO_2-SiO_2	160	2.5	12	22.9	H_2O	96	81.6	1.6	[23]
10C-2G [c]	180	1	5	19.6	Methanol	100	99	81.7	[24]
Co@NC-700	180	FA	4	12.7	H_2O	95.7	95.7	3.0	[25]
Ni/CCNTs-4	190	1	5	38.6	H_2O + Methanol	90	78.9	6.1	[26]

[a] Turnover frequency (TOF) = (total number of designed products moles per hour)/(total number moles of active metal). [b] TOF = (total number of designed products moles per hour)/(total number moles of active metal × metal dispersion (%)). [c] TOF = (total number of reactant moles converted per hour)/(total number moles of active metal × metal dispersion (%)), the conversion of vanillin is less than 10%. [d] S/C represents the molar ratio of substrate to metal.

Table S6. BET surface areas and pore structure parameters of Cu-based samples

Entry	Materials	S_{BET} (m^2/g)	Pore Size (nm) [a]	Pore Volume (cm^3/g) [b]
1	SiO_2	1011	2.4	0.56
4	Cu/SiO_2-IM	875.4	2.7	0.52
5	Cu/SiO_2-AE	640.1	5.4	1.03
6	Cu/SiO_2-AEH	443.9	6.1	0.77

[a] BJH Desorption average pore diameter; [b] BJH Desorption cumulative volume.

Table S7. Characterization of active metal Cu in obtained catalysts.

Entry	Materials	W_{Cu} (wt%) [a]	D_{Cu} (nm) [b]	D_p (%) [c]
1	Cu/SiO_2-IM	11.7	15.1	10.6
1	Cu/SiO_2-AE	8.6	1.8	50.3
2	Cu/SiO_2-AEH	8.4	2.6	40.1
3	Cu/SiO_2-AE-5 runs	5.3	2.0	38.2
4	Cu/SiO_2-AEH-5 runs	7.3	2.6	31.1

[a] The actual loading of Cu was measured by ICP-AES; [b] The particle size of Cu was calculated by TEM images; [c] The dispersion of Cu was measured by N_2O surface oxidation.

References

1. Tan J, Xia X, Cui J, Yan W, Jiang Z, Zhao Y. Efficient Tuning of Surface Nickel Species of the Ni-Phyllosilicate Catalyst for the Hydrogenation of Maleic Anhydride. *J. Phys. Chem. C* **2019**, *123*, 9779-9787, doi:10.1021/acs.jpcc.8b11972.
2. Feng Y, Yin H, Wang A, Xie T, Jiang T. Selective hydrogenation of maleic anhydride to succinic anhydride catalyzed by metallic nickel catalysts. *Appl. Catal. A* **2012**, *425-426*, 205-212, doi:10.1016/j.apcata.2012.03.023.
3. Pillai UR, Sahle-Demessie E, Young D. Maleic anhydride hydrogenation over Pd/Al_2O_3 catalyst under supercritical CO_2 medium. *Appl. Catal. B* **2003**, *43*, 131-138, doi:10.1016/s0926-3373(02)00305-3.
4. Torres CC, Alderete JB, Mella C, Pawelec B. Maleic anhydride hydrogenation to succinic anhydride over mesoporous Ni/TiO_2 catalysts: Effects of Ni loading and temperature. *J. Mol. Catal. A Chem.* **2016**, *423*, 441-448, doi:10.1016/j.molcata.2016.07.037.
5. Gao C, Zhao Y, Liu D. Liquid phase hydrogenation of maleic anhydride over nickel catalyst supported on ZrO_2–SiO_2 composite aerogels. *Catal. Lett.* **2007**, *118*, 50-54, doi:10.1007/s10562-007-9135-4.
6. Tang C, Liu Y, Xu C, Zhu J, Wei X, Zhou L, et al. Ultrafine Nickel-Nanoparticle-Enabled SiO_2 Hierarchical Hollow Spheres for High-Performance Lithium Storage. *Adv. Funct. Mater.* **2018**, *28*, 1704561, doi:10.1002/adfm.201704561.
7. Liao X, Zhang Y, Guo J, Zhao L, Hill M, Jiang Z, et al. The Catalytic Hydrogenation of Maleic Anhydride on $CeO_{2-\delta}$-Supported Transition Metal Catalysts. *Catalysts* **2017**, *7*, 272, doi:10.3390/catal7090272.
8. Zhao L, Zhao J, Wu T, Zhao M, Yan W, Zhang Y, et al. Synergistic Effect of Oxygen Vacancies and Ni Species on Tuning Selectivity of Ni/ZrO_2 Catalyst for Hydrogenation of Maleic Anhydride into Succinic Anhydride and gamma-Butyrolacetone. *Nanomaterials* **2019**, *9*, 406, doi:10.3390/nano9030406.
9. Liao X, Zhang Y, Hill M, Xia X, Zhao Y, Jiang Z. Highly efficient Ni/CeO_2 catalyst for the liquid phase hydrogenation of maleic anhydride. *Appl. Catal. A* **2014**, *488*, 256-264, doi:10.1016/j.apcata.2014.09.042.
10. Jeong H, Hwan Kim T, Ill Kim K, Haeng Cho S. The hydrogenation of maleic anhydride to γ-butyrolactone using mixed metal oxide catalysts in a batch-type reactor. *Fuel Process. Technol.* **2006**, *87*, 497-503, doi:10.1016/j.fuproc.2005.11.007.
11. Jung SM, Godard E, Jung SY, Park KC, Choi JU. Liquid-phase hydrogenation of maleic anhydride over Pd/SiO_2: effect of tin on catalytic activity and deactivation. *J. Mol. Catal. A Chem.* **2003**, *198*, 297-302, doi:10.1016/s1381-1169(02)00686-6.
12. Fan R, Hu Z, Chen C, Zhu X, Zhang H, Zhang Y, et al. Highly dispersed nickel anchored on a N-doped carbon molecular sieve derived from metal-organic frameworks for efficient hydrodeoxygenation in the aqueous phase. *Chem. Commun.* **2020**, *56*, 6696-6699, doi:10.1039/d0cc02620d.
13. Li M, Deng J, Lan Y, Wang Y. Efficient Catalytic Hydrodeoxygenation of Aromatic Carbonyls over a Nitrogen-Doped Hierarchical Porous Carbon Supported Nickel Catalyst. *ChemistrySelect* **2017**, *2*, 8486-8492, doi:10.1002/slct.201701950.
14. Fan R, Chen C, Han M, Gong W, Zhang H, Zhang Y, et al. Highly Dispersed Copper Nanoparticles Supported on Activated Carbon as an Efficient Catalyst for Selective Reduction of Vanillin. *Small* **2018**, *14*, e1801953, doi:10.1002/smll.201801953.
15. Yue X, Zhang L, Sun L, Gao S, Gao W, Cheng X, et al. Highly efficient hydrodeoxygenation of lignin-derivatives over Ni-based catalyst. *Appl. Catal. B* **2021**, *293*, 120243, doi:10.1016/j.apcatb.2021.120243.
16. Zhang L, Shang N, Gao S, Wang J, Meng T, Du C, et al. Atomically Dispersed Co Catalyst for Efficient Hydrodeoxygenation of Lignin-Derived Species and Hydrogenation of Nitroaromatics. *ACS Catal.* **2020**, *10*, 8672-8682, doi:10.1021/acscatal.0c00239.
17. Zhang X, Zhang Z, Li H. Enhanced Effect of Carbon for the $Ni/T\text{-}Nb_2O_5$ Catalyst on Vanillin

Hydrodeoxygenation in the Aqueous Phase. *Energy Fuel.* **2024**, *38*, 8726-8739, doi:10.1021/acs.energyfuels.3c04354.
18. Du K, Li H, Jiang L, Xu K, Xu J, Wang Y, et al. Interface enhanced catalytic hydrodeoxygenation of vanillin as a bio-oil model using Ni-based catalysts. *Chem. Eng. J.* **2025**, *520*, 166037, doi:10.1016/j.cej.2025.166037.
19. Liu M, Zhang J, Zheng L, Fan G, Yang L, Li F. Significant Promotion of Surface Oxygen Vacancies on Bimetallic CoNi Nanocatalysts for Hydrodeoxygenation of Biomass-derived Vanillin to Produce Methylcyclohexanol. *ACS Sustain. Chem. Eng.* **2020**, *8*, 6075-6089, doi:10.1021/acssuschemeng.0c01015.
20. Nie R, Yang H, Zhang H, Yu X, Lu X, Zhou D, et al. Mild-temperature hydrodeoxygenation of vanillin over porous nitrogen-doped carbon black supported nickel nanoparticles. *Green Chem.* **2017**, *19*, 3126-3134, doi:10.1039/c7gc00531h.
21. Zhao TJ, Zhang JJ, Wang HH, Su J, Li XH, Chen JS. Biomimetic Design of a 3D Transition Metal/Carbon Dyad for the One-Step Hydrodeoxygenation of Vanillin. *ChemSusChem* **2020**, *13*, 1900-1905, doi:10.1002/cssc.201902937.
22. Shit SC, Koley P, Joseph B, Marini C, Nakka L, Tardio J, et al. Porous Organic Polymer-Driven Evolution of High-Performance Cobalt Phosphide Hybrid Nanosheets as Vanillin Hydrodeoxygenation Catalyst. *ACS Appl. Mater. Interfaces* **2019**, *11*, 24140-24153, doi:10.1021/acsami.9b06789.
23. Mukherjee D, Singuru R, Venkataswamy P, Damma D, Reddy BM. Ceria Promoted Cu-Ni/SiO_2 Catalyst for Selective Hydrodeoxygenation of Vanillin. *ACS Omega* **2019**, *4*, 4770-4778, doi:10.1021/acsomega.9b00039.
24. Verma D, Insyani R, Cahyadi HS, Park J, Kim SM, Cho JM, et al. Ga-doped Cu/H-nanozeolite-Y catalyst for selective hydrogenation and hydrodeoxygenation of lignin-derived chemicals. *Green Chem.* **2018**, *20*, 3253-3270, doi:10.1039/c8gc00629f.
25. Yang H, Nie R, Xia W, Yu X, Jin D, Lu X, et al. Co embedded within biomass-derived mesoporous N-doped carbon as an acid-resistant and chemoselective catalyst for transfer hydrodeoxygenation of biomass with formic acid. *Green Chem.* **2017**, *19*, 5714-5722, doi:10.1039/c7gc02648j.
26. Li H, Liu Z. Hydrodeoxygenation of vanillin as model compound for pyrolysis oil over carboxylic carbon nanotubes-supported Ni catalysts. *Bioresour. Technol.* **2019**, *5*, 86-90, doi:10.1016/j.biteb.2018.12.001.